#### **Research Article**

Humaira Yasmin\*, Showkat Ahmad Lone, Farhan Ali, Hussam Alrabaiah, Zehba Raizah, and Anwar Saeed\*

# Thermal radiative flow of cross nanofluid due to a stretched cylinder containing microorganisms

https://doi.org/10.1515/ntrev-2023-0147 received August 13, 2023; accepted October 11, 2023

**Abstract:** Due to its widespread applications in areas including heat exchangers, cancer therapy, heat storage devices, biomedicine, and biotechnology, nanofluid has become one of the most important fluids in thermal engineering. One difficulty with these applications of nanofluids is the improvement of heat conductivity via nanoparticles. This aims to illustrate the bioconvectional cross-flow of a nanofluid in the existence of swimming gyrotactic microorganisms over a vertical stretching cylinder. We consider the chemical reaction and thermal radiation in the energy and concentration equations. Through the use of appropriate dimensionless variables, a nonlinear system of partial differential equations has been transformed into ordinary differential equations (ODEs). The BVP4c method is applied to construct the resultant governing ODEs. The significance of physical variables is demonstrated through plots and tabular data. Our finding explains that the temperature intensifies due to larger curvature parameters and Weissenberg variables, while the opposite effect is examined in the velocity profile. With upsurge in thermophoresis parameter, the temperature upsurges accordingly. As the bioconvection Lewis

number rises, microbial concentration falls. The results obtained in this investigation could be useful in practical applications like numerous areas of engineering, biotechnology, nanotechnology, and medical sciences *etc*.

**Keywords:** cross-fluid, nanofluid, stretching cylinder, bioconvection flow, thermal radiation, convective flow

#### **Abbreviations**

We	Weissenberg p	arameter
----	---------------	----------

Rm bioconvection Rayleigh number

Nc buoyancy parameter

 $B_{\rm i}$  biot number

Nb brownian motion

Nt thermophoresis force

Pr Prandtl number

Rd radiation parameter

*K*\* mean absorption

Sc Schmidt number

F' radial velocity

 $\vartheta$  temperature field

 $\Pi$  concentration field

Y microorganism field

au ratio of effective heat capacity

 $\kappa$  chemical reaction

Pe Peclet number

Lb bioconvection Lewis number

 $\omega$  microorganism concentration difference

Cf skin friction coefficient

Nu<sub>r</sub> Nusselt number

Sh<sub>r</sub> Sherwood number

Nh motile density

*u*, *v* component of velocity

 $\delta$  curvature parameter

 $\lambda$  mixed convective parameter

 $c_{\rm p}$  specific heat

g acceleration due to gravity

 $\mu_{\rm f}$  dynamic visocisty

 $v_{
m f}$  kinematic viscosity of EG

<sup>\*</sup> Corresponding author: Humaira Yasmin, Department of Basic Sciences, General Administration of the Preparatory Year, King Faisal University, 31982, Al Ahsa, Saudi Arabia, e-mail: hhassain@kfu.edu.sa

<sup>\*</sup> Corresponding author: Anwar Saeed, Department of Mathematics, Abdul Wali Khan University, Mardan, 23200, Khyber Pakhtunkhwa, Pakistan, e-mail: anwarsaeed769@gmail.com

**Showkat Ahmad Lone:** Department of Basic Sciences, College of Science and Theoretical Studies, Saudi Electronic University, Jeddah-M, Riyadh 11673, Saudi Arabia

**Farhan Ali:** Department of Mathematical Sciences, Federal Urdu University of Arts, Sciences & Technology, Gulshan-e-Iqbal, 75300, Karachi. Pakistan

**Hussam Alrabaiah:** College of Engineering, Al Ain University, Al Ain, United Arab Emirates; Mathematics Department, Tafila Technical University, Tafila, Jordan

**Zehba Raizah:** Department of Mathematics, College of Science, Abha, King Khalid University, Saudi Arabia

2 — Humaira Yasmin et al. DE GRUYTER

 $\alpha_{\mathrm{f}}$ thermal diffusivity kinematic viscosity of EG  $v_{\rm f}$ thermal diffusivity  $\alpha_{\rm f}$ k thermal conductivity nanofluid density  $\rho_{\rm f}$ microorganism particles density  $\rho_{\rm m}$ Brownian diffusion coefficient  $D_{\mathrm{B}}$  $D_{\mathrm{T}}$ thermophoretic diffusion coefficient  $D_{\rm M}$ microorganism diffusion coefficient  $\sigma^*$ Stefan-Boltzmann constant T temperature of the fluid  $T_{w}$ wall temperature  $T_{\infty}$ ambient temperature

 $T_{\rm f}$  surface heat

*h* coefficient of heat transfer

 $Y_{\rm w}$  surface concentration of microorganisms  $Y_{\infty}$  ambient concentration of microorganisms

 $q_{\rm r}$  radiative heat flux

## 1 Introduction

Cross-fluid flow over a stretched cylinder describes the movement of a fluid across the surface of a cylindrical object that is undergoing stretching or elongation. This phenomenon is encountered in various practical applications, such as the coating process in manufacturing, polymer processing, and fiber spinning. When a cylinder is stretched, the fluid on its surface experiences both tangential and normal forces. The tangential forces arise due to the stretching motion, causing the fluid to move along the surface. The normal forces act perpendicular to the surface and induce a cross-flow across the cylinder. This cross-flow is characterized by fluid moving from one side of the cylinder to the other. The flow behavior of the fluid on a stretching cylinder contains several influences, including the velocity of stretching, the viscosity of the fluid, and the surface properties of the cylinder [1,2]. As the stretching velocity increases, the crossflow becomes more pronounced [3]. Higher fluid viscosity tends to resist the cross-flow, while lower viscosity promotes it. The surface properties of the cylinder, such as its roughness or surface tension, can also influence the cross-flow behavior [4]. By gaining a deeper understanding of cross-fluid flow on a stretching cylinder, engineers develop more efficient processes, improve product quality, and optimize material usage in various industrial applications [5]. Khan et al. [6] evaluated computationally the thermal transportation for cross-flow of Williamson fluid on an elongating and contracting surface using thermally radiative effects. Khosravi and Javan [7] discussed 3D thermal transportation considering deep cross-flow

using mesh refinement. Understanding the dynamics of cross-fluid flow on a stretching cylinder is essential for optimizing processes that involve the coating or spreading of materials [8]. Darvesh *et al.* [9] examined the 3D cross-flow of nanofluid using the density of microorganisms and noted that a slight change in the Brownian motion parameter has a significant impact on the concentration of nanoparticles and motile microorganisms. They have also shown that there was an approximately 80.21% reduction in the concentration as a result of the slight modification in the Brownian movement variable.

Nanofluid flow describes the motion of a mixture of nanoparticles and a base fluid. A nanofluid consists of solid nanoparticles, typically in the range of 1-100 nm, dispersed in a liquid medium. This combination of nanoparticles and fluid exhibits unique flow characteristics and properties compared to pure fluids as introduced initially by Choi and Eastman [10]. When nanofluids flow, the nanoparticles interact with the base fluid, leading to alterations in the overall fluid behavior [11]. These interactions can affect various flow parameters such as viscosity, thermal conductivity, density, and heat transfer capabilities. Consequently, nanofluid flow has garnered significant interest in several fields, including engineering, materials science, and energy applications. One crucial aspect of nanofluid flow is the enhanced thermal conductivity [12]. Nanoparticles, due to their larger surface area-to-volume ratio, can significantly improve the thermal properties of the base fluid when dispersed [13]. As a result, nanofluids have been explored for features such as heat transport enhancement in cooling systems, thermal executive of electronic devices, and solar thermal collectors. The flow behavior of nanofluids is influenced by factors such as nanoparticle concentration, size, shape, and surface characteristics [14]. These parameters can affect the stability and dispersion of nanoparticles within the fluid medium, leading to variations in the flow properties. Understanding the flow dynamics of nanofluids helps in optimizing their usage in different applications and designing efficient heat transfer systems [15]. Nanofluid flow has proved to have potential in various fields, including heat exchangers, microfluidics, biomedical engineering, and energy conversion systems [16]. Khan et al. [17] studied thermally the blood-gold nanofluid flow on a surface through the impacts of microorganisms and noted that thermal panels were reinforced by intensification in thermophoresis factor, volumetric fraction, Brownian movement, and radiation variables, as they were opposite via the Prandtl number. The fluid concentration augmented through an upsurge in activation energy parameters and decayed on boost in thermophoresis factor and the Schmidt number. Many investigations are witnessed of nanofluid flow on cylindrical surfaces with a remarkable contribution to the thermal flow analysis [18]. Bhatti and Ellahi [19] studied computationally the nanofluid non-Darcian flow on an elastic as well as elongating surface using thermal and velocity slips.

As the fluid flows over the cylinder, a boundary layer forms near its surface. In the stretching cylinder, the boundary layer can undergo separation, where it lifts off the surface. The occurrence of boundary layer separation is influenced by the stretching rate and fluid viscosity [20]. The separation of the boundary layer has significant consequences for the flow behavior, including changes in pressure distribution and drag forces. The stretching of the cylinder can induce a transition from laminar to turbulent flow [21]. The critical Reynolds number for this transition depends on factors such as the stretching rate, surface roughness, and fluid properties. Turbulent flow typically exhibits higher drag forces compared to laminar flow. The stretching of the cylinder can also cause changes in the flow velocity; in some cases, the fluid can be accelerated along the cylinder's surface, resulting in increased flow rates [22]. However, depending on the stretching rate and other factors, the fluid can also decelerate as it moves along the cylinder. Reddy et al. [23] discussed thermal generation and absorption for nanofluid magnetohydrodynamics (MHD) flow on a stretch cylinder through a porous surface and noted that growth in the curvature and the porosity factors are expected to amplify the thermal layer within the boundary layer region surrounding the cylinder. Othman et al. [24] simulated computationally the flow of nanoparticles in combination with microorganisms and activated energy on an elongating and inclined cylinder and have observed that inclination angle and Richardson number have been observed to cause a reduction in the velocity curve, while it has boosted in response to changes in the curvature factor. They have also noted that the energy field is enhanced by the inclination angle and heat source term, but it has diminished through the Prandtl number and Richardson number. Shaheen et al. [25] discussed time-dependent bio-convective fluid flow on an elongating cylinder under the impact of different flow constraints.

Bio-convection flow discusses the convective motion of a fluid induced by the collective movement of microorganisms or biological entities within the fluid. This phenomenon is commonly observed in various biological systems, such as suspensions of swimming bacteria, algae, or other microorganisms [26]. Bio-convection arises due to the inherent biological activity of these organisms, which can result in the generation of concentration gradients or localized heating [27]. These gradients lead to buoyancy forces that drive fluid motion. The collective movement of microorganisms, typically driven by their motility mechanisms, can create vortices, flow patterns, and instabilities in the fluid flow [28]. In research and scientific studies, bio-convection flow has been investigated to understand various biological and ecological processes [29]. It plays a significant role in diverse fields, including microbiology, ecology, biophysics, and bioengineering. Saraswathy et al. [30] studied theoretically the bio-convective fluid flow over a sheet by incorporating the effects of heat and mass flux models proposed by Cattaneo-Christov and have noted that their results have been in remarkable agreement with established data. Chu et al. [31] explored the significance of bio-convection with activation energy on the magnetic field on a stretching surface through the famous Buonigiorno model and noted that velocity distribution has declined while thermal panels are amplified and grow. Hussain et al. [32] inspected the impact of bio-convection using microorganisms on a fluid layer through two infinite plates with gravitational effects.

Fluid flow with the effect of thermal radiative encompasses a complex relation between fluid dynamics and heat transfer. When thermal radiation is considered in a flow system, it introduces an additional mode of heat transfer alongside conduction and convection [33]. Unlike conduction and convection, which require a material medium, thermal radiation involves the emission, absorption, and transmission of electromagnetic waves. Radiative heat transfer plays a crucial role in influencing the energy balance and temperature distribution within the flow system [34]. The amount of heat transfer through radiation depends on the temperature and emissivity of the surfaces involved. It can lead to both heating and cooling effects, depending on the temperature gradient and emissivity distribution. The absorption and emission of radiation by the fluid and solid surfaces within the flow system significantly impact the overall energy exchange. The absorption of radiation by the fluid can increase its temperature, while the emission of radiation from the fluid and solid surfaces affects the overall heat transfer. The emissivity and absorptivity of the surfaces determine the extent of these interactions. To analyze fluid flow with the effects of thermal radiation, mathematical models such as the radiative transfer equation are employed [35]. These models incorporate the radiative heat transfer mechanisms and interactions within the system, allowing for predicting temperature distributions, flow patterns, and overall system behavior. Dharmaiah et al. [36] applied Jeffery MHD fluid flow factor to the nuclear reactor with Brownian motion and thermophoresis effects and thermal radiations on a wedge and noted that

fluid velocity panels have reduced and thermal panels have boosted with growth in magnetic factor. Suresh Kumar et al. [37] analyzed computationally the MHD fluid flow with impacts of microorganisms and thermally radiative effects and Hall current. Pandev et al. [38] discussed the relation between thermal radiations with mixed convection for a fluid flow on a stretching surface. Alrehili [39] analyzed the upgradation of applications regarding the field of engineering and technology for dissipative nanofluid flow on a nonlinear elongating sheet using thermally radiative effects. Sharma et al. [40] studied the generation of entropy and thermally radiative effects for Jeffery electro magnetohydrodynamics fluid flow with impacts of nanoparticles and have noted that velocity distribution has retarded while thermal panels have boosted with growth in magnetic factor and concentration of nanoparticles.

When a force is applied to a fluid, the fluid undergoes a deformation or a change in shape or structure. Non-Newtonian fluids include things such as toothpaste, ketchup, paint, blood, starch, and so forth, while Newtonian fluids have a linear relationship between applied force and deformation. There are a wide variety of mathematical models available for investigating the characteristics of these non-Newtonian fluids. Many models have been proposed to explain fluid behavior, including Burger's, Jeffery's, Ree-Eyring, Power law, and many others. Cross [41] used the cross-fluid model to represent the characteristics of any fluid at both high and low shear rates. Rehman et al. [42] explained the force convection flow subject to the effect of thermal diffusion and mass diffusion with crossflow through a variable needle. Azam et al. [43] examined the solar aspect of the magnetic flow of cross nanofluid due to convective flow. Yao et al. [44] investigated the impact of an orthogonal magnetic dipole on cross-fluid, which exhibits numerous characteristics. Khan et al. [45] illustrated the activation energy and thermophoretic effect on cross-fluid. Sharma and Mishra [46] provided an interpretation of the higher-order mechanism of chemical reaction and the effect of Lorentz force on cross-fluid.

The main aim of this analysis is to examine the cross-nanofluid flow caused by cylinder's stretching. Because of the presence of mixed convection, it is presumed that the flow is vertical. Based on the aforementioned review of the literature and to the best of the author's knowledge, no research has been done on the interaction of cross-nanomaterial with microorganisms. As a result, closing this gap is the primary focus of our argument. So, our investigation explains the cross fluid in the presence of thermal radiative, mixed convective flow, and microorganisms. Convective boundary conditions are imposed along with impacts of Brownian motion and thermophoresis motile microorganisms. In this work, we used the Byp4c technique to calculate

the numerical solutions. Plots are also elaborated to interpret the features of other physical variables.

## 2 Modeled formulation

We investigate the 2D cross-mixed convective flow of an incompressible viscoelastic nanoliquid comprising chemical reaction and convective condition on a stretched cylinder, taking into account the effects of thermal radiation, as shown in Figure 1. The symbols  $T_{\infty}$ ,  $C_{\infty}$ , and  $Y_{\infty}$ , respectively, represent the temperature, the concentration, and concentration of microorganism at free stream. The physical nature of the model is outlined below.

Therefore, the constitutive equation of the flow model expression is described as follows [43–45]:

$$\frac{\partial ru}{\partial x} + \frac{\partial rv}{\partial r} = 0,\tag{1}$$

$$u\frac{\partial u}{\partial x} + v\frac{\partial u}{\partial r}$$

$$= v_{f}\frac{\partial u}{\partial r} \left[ \left[ \frac{1}{1 + \left[ \Gamma \frac{\partial u}{\partial y} \right]^{n}} \right] + \frac{v_{f}}{r} \frac{\partial}{\partial r} \left[ \left[ \frac{\frac{\partial u}{\partial r}}{1 + \left[ \Gamma \frac{\partial u}{\partial y} \right]^{n}} \right] \right] + ((1 - \Phi_{\infty})\rho_{f}\beta(T - T_{\infty}) - (\rho_{p} - \rho_{f})g(C - C_{\infty}) - \gamma(\rho_{m} - \rho_{f})g(Y - Y_{\infty})),$$

$$(2)$$

$$u\frac{\partial T}{\partial x} + v\frac{\partial T}{\partial r} - \left[ a_{\rm f} + \frac{16\sigma^* T_{\infty}^3}{3k(\rho C_{\rm p})_{\rm f}} \right] \left( \frac{\partial^2 T}{\partial r^2} + \frac{1}{r} \frac{\partial T}{\partial r} \right)$$

$$= \tau \left[ D_{\rm B} \frac{\partial C}{\partial r} \frac{\partial T}{\partial r} + \frac{D_{\rm T}}{T_{\infty}} \left( \frac{\partial T}{\partial r} \right)^2 \right] + \frac{Q_0}{(\rho C_{\rm p})_{\rm f}} (T - T_{\infty}),$$
(3)

$$u\frac{\partial C}{\partial x} + v\frac{\partial C}{\partial r} = D_B \left[ \frac{1}{r} \frac{\partial C}{\partial r} + \frac{\partial^2 C}{\partial r^2} \right] + \frac{D_T}{T_\infty} \left[ \frac{\partial^2 T}{\partial r^2} + \frac{1}{r} \frac{\partial T}{\partial r} \right]$$
(4)
$$- K_0 (C - C_\infty),$$

$$u\frac{\partial Y}{\partial x} + v\frac{\partial Y}{\partial r} + \frac{bW_{\rm c}}{(C_{\rm w} - C_{\infty})} \frac{1}{r} \left( \frac{\partial}{\partial r} \left[ Y \frac{\partial C}{\partial r} \right] \right) = D_{\rm m} \frac{\partial^2 Y}{\partial r^2}.$$
 (5)

The boundary constraints are applied as follows [43-45]:

$$u = \frac{u_0}{l}X, v = 0, -k\frac{\partial T}{\partial r} = h(T_f - T), C = C_w,$$

$$Y = Y_w \quad \text{at} \quad r = R,$$

$$u \to 0, T \to T_\infty, C \to C_\infty, Y \to Y_\infty \quad \text{as} \quad r \to \infty,$$
(6)

where u and v represent the velocity component along the x- and r-axis.  $\Gamma$  is represented by the relaxation time, n is the power index,  $\rho_f$  is the density of the fluid,  $\rho_n$  describes

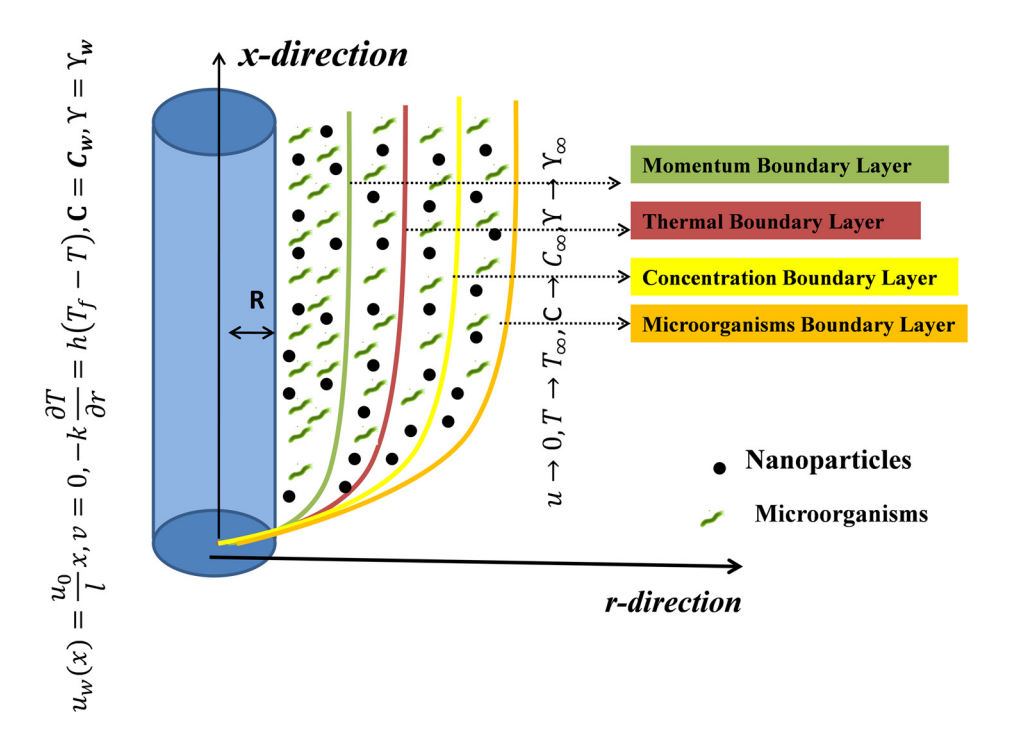


Figure 1: Geometry of the flow problem.

the density of nanoparticles,  $\rho_{\rm m}$  denotes the density of microorganisms,  $(\rho C_{\rm p})_{\rm f}$  denotes the specific heat capacity of the fluid, T is the temperature of the fluid,  $D_{\rm m}$  describes microorganism diffusion,  $bW_{\rm c}$  displays cell's swimming speed,  $D_{\rm B}$  defines the thermophoretic diffusion,  $\tau$  is defined as the heat capacity ratio of nanofluid,  $v_{\rm f}$  defines as the kinematics viscosity, and  $\mu$  defines the dynamic viscosity.

Similarity transformation is [43-45]

+ PrNt $\vartheta'^2 = 0$ ,

$$\xi = \sqrt{\frac{u_{0}}{v_{f}l}} \left( \frac{r^{2} - R^{2}}{2R} \right), u = \frac{u_{0}x}{l} F'(\xi), v = -\frac{R}{r} \sqrt{\frac{u_{0}v_{f}}{l}} F(\xi),$$

$$\vartheta(\xi) = \frac{T - T_{\infty}}{T_{f} - T_{\infty}}, \Phi(\xi) = \frac{C - C_{\infty}}{C_{W} - C_{\infty}}, \Pi(\xi) = \frac{Y - Y_{\infty}}{Y_{W} - Y_{\infty}}.$$
(7)

After applying above-mentioned transformation to equations (2)–(6), the nonlinear dimensionless ordinary differential equations (ODEs) are obtained as follows:

$$(1 + 2\delta\xi)[(1 + (1 - n)(WeF'')^n)F''']$$

$$+ 2\delta F'' \left[ \left[ 1 + \left[ 1 - \frac{n}{2} \right] (WeF'')^n \right] \right]$$

$$+ [FF'' - F'^2] \{ 1 + (WeF'')^n \}^2 + \delta^2 \lambda (\vartheta - Nc\Phi - Rm\Pi) \{ 1 + (WeF'')^n \}^2 = 0,$$

$$\vartheta'' (1 + 2\delta\xi) \left[ 1 + \frac{4}{3} Rd \right] + \delta\vartheta' + PrF\vartheta' + PrNb\vartheta'\Phi'$$
(9)

$$\Phi''(1+2\delta\xi) + \delta\Phi' + \text{Sc}F\Phi' + \frac{\text{Nt}}{\text{Nb}}[(1+2\delta\xi)\vartheta'' + \delta\Phi'] - \text{Sc}\delta\Phi = 0,$$
(10)

$$\Pi^{''}(1+2\delta\xi) + \delta\Pi' + \text{Lb}F\Pi' - \text{Pe}[\Pi'\Phi' + (1+\delta\xi)\Phi^{''} + \delta\Phi')(\Pi+\omega)]. \tag{11}$$

Subject to the boundary conditions

$$F(0) = 0, F'(0) = 1, \vartheta'(0) = -B_i(1 - \vartheta(0)),$$
  

$$\Phi(0) = 1, \Pi(0) = 1 \text{ as } \xi = 0$$
. (12)  

$$F' \to 0, \vartheta \to 0, \Phi \to 0, \Pi \to 0 \text{ as } \xi \to \infty,$$

where We is the Weissenberg number,  $\delta$  denotes the curvature variable,  $\lambda$  denotes the mixed convective parameter, Nc represents the buoyancy parameter, Rm denotes the bioconvection Rayleigh number, Pr denotes the Prandtl number,

Nb denotes the Brownian motion, Sc is the Schmidt number, Nt is the thermophoretic diffusion, Lb denotes the bioconvection Lewis number, Pe denotes the Peclet number,  $\omega$  denotes the microorganism difference, Bi denotes the Biot number, and Rd exhibits the thermal radiation factor

We = 
$$\left(\frac{\Gamma u_0}{l}\right)^{1/2} \text{Re}_x^{1/2}$$
,  $\delta = \left(\frac{v_f l}{u_0 R^2}\right)^{1/2}$ ,  
 $\lambda = \frac{(1 - C_f)(T_f - T_\infty)\beta g}{z\left(\frac{u_0}{l}\right)^2}$ , Nc =  $\frac{(\rho_p - \rho_f)(C_w - C_\infty)}{\beta(1 - C_f)(T_f - T_\infty)\rho_f}$ 

6 — Humaira Yasmin et al. DE GRUYTER

$$\operatorname{Rm} = \frac{(\rho_{\mathrm{m}} - \rho_{\mathrm{f}})(Y_{\mathrm{W}} - Y_{\infty})\gamma}{\beta(1 - C_{\mathrm{f}})(T_{\mathrm{f}} - T_{\infty})\rho_{\mathrm{f}}}, \operatorname{Pr} = \frac{C_{\mathrm{p}}}{k}, \operatorname{Nb} = \frac{\tau D_{\mathrm{B}}(C_{\mathrm{W}} - C_{\infty})}{v_{\mathrm{f}}},$$

$$\operatorname{Sc} = \frac{v_{\mathrm{f}}}{D_{\mathrm{B}}}, \operatorname{Nt} = \frac{\tau D_{\mathrm{T}}(T_{\mathrm{f}} - T_{\infty})}{v_{\mathrm{f}}T_{\infty}},$$

$$\operatorname{Lb} = \frac{v_{\mathrm{f}}}{D_{\mathrm{m}}}, \operatorname{Pe} = \frac{bWc}{D_{\mathrm{m}}}, \omega = \frac{Y_{\infty}}{Y_{\mathrm{W}} - Y_{\infty}}, B_{i} = \frac{h}{k} \sqrt{\frac{v_{\mathrm{f}} I}{u_{\mathrm{o}}}},$$

$$\operatorname{Rd} = \frac{4\sigma^{*}T_{\infty}^{3}}{kk^{*}}.$$

Engineering quantities of interest are [43-45]

$$C_{f} = \frac{\tau_{xr}}{\rho_{F}U_{W}^{2}},$$

$$Nu = \frac{xq_{w}}{k(T_{f} - T_{\infty})},$$

$$Sh = \frac{xq_{m}}{D_{B}(C_{w} - C_{\infty})},$$

$$Nh = \frac{xq_{n}}{D_{m}(Y_{w} - Y_{\infty})}.$$
(13)

 $\tau_{\rm xr}$ ,  $q_{\rm w}$ ,  $q_{\rm m}$ , and  $q_{\rm n}$  are described as follows:

$$\tau_{xr} = \mu_0 \frac{\partial u}{\partial r} \left[ \frac{1}{1 + \left[ \Gamma \frac{\partial u}{\partial r} \right]^n} \right]$$

$$q_w = -k \left[ 1 + \frac{4}{3} \operatorname{Rd} \right] \frac{\partial T}{\partial r},$$

$$q_m = -D_B \frac{\partial C}{\partial r},$$

$$q_n = -D_m \frac{\partial Y}{\partial r}.$$
(14)

Using similarity transformation to equation (14), we obtain

Cf Re<sup>1/2</sup> = 
$$F''(0) \left[ \frac{1}{1 + (WeF''(0))^n} \right],$$
  
Nu Re<sup>-1/2</sup> =  $-\vartheta'(0) \left[ 1 + \frac{4}{3} \text{Rd} \right],$   
Sh Re<sup>-1/2</sup> =  $-\Phi'(0),$   
Nh Re<sup>-1/2</sup> =  $-\Pi'(0),$ 

where  $Re_x = xU_w/v_F$  is the local Reynolds number.

# 2.1 Numerical procedure

It is vital to compute the technique after reducing the problem to a lower order. Examining the given equations shows their highly nonlinear nature, posing challenges in maintaining analytical expressions. Initially, the conditions are estimated using a shooting approach. To achieve this, we utilize the finite difference technique with the bvp4c code in computer models and simulations. With these assumptions, we are able to convert the initial problem into a first-order system

$$F = A_{1}, F' = A_{2}, F'' = A_{3}, F''' = A'_{3}$$

$$\vartheta = A_{4}, \vartheta' = A_{5}, \vartheta'' = A'_{5}$$

$$\Phi = A_{6}, \Phi' = A_{7}, \Phi'' = A'_{7},$$

$$\Pi = A_{8}, \Pi' = A_{9}, \Pi'' = A'_{9},$$
(16)

$$A_{3}' = \frac{-2\alpha A_{3} \left[ \left[ 1 + \left[ 1 - \frac{n}{2} \right] (WeA_{3})^{n} \right] \right] - [A_{1}A_{3} - (A_{2})^{2}] \{ 1 + (WeA_{3})^{n} \}^{2} - \delta^{2} \lambda (A_{4} - NcA_{6} - RmA_{8}) \{ 1 + (WeA_{3})^{n} \}^{2}}{(1 + 2\delta \xi)(1 + (1 - n)(WeA_{3})^{n})},$$

$$(17)$$

$$A_{5}' = \frac{-\delta A_{5} - \text{Pr}A_{1}A_{5} - \text{Pr}\text{Nb}A_{5}A_{7} - \text{Pr}\text{Nt}A_{5}^{2}}{(1 + 2\delta\xi)(1 + \frac{4}{3}\text{Rd})},$$
(18)

$$A_7' = \frac{-\delta A_7 - \text{Sc} A_1 A_5 - \frac{\text{Nt}}{\text{Nb}} [(1 + 2\delta \xi) A_5' + \delta A_7] - \text{Sc} \delta A_7}{(1 + 2\delta \xi)},$$
(19)

$$A_{9}' = \frac{-\delta A_{9} - \text{Lb} A_{1} A_{9} + \text{Pe}[A_{7} A_{9} + (1 + \delta \xi) A_{7}' + \delta A_{7}) (A_{8} + \omega)]}{(1 + 2\delta \xi)}.$$
 (20)

Subject to the boundary conditions

$$A_{1} = 0, A_{2} = 1, A_{5} = -B_{i}(1 - A_{4}), A_{6} = 1,$$

$$A_{8} = 1 \quad \text{as} \quad \xi = 0$$

$$A_{2} \rightarrow 0, A_{4} \rightarrow 0, A_{6} \rightarrow 0, A_{8} \rightarrow 0 \quad \text{as} \quad \xi \rightarrow 0.$$
(21)

# 3 Results and discussion

This portion comprised the mechanism of various physical factors' impacts on profiles  $F'(\xi), \vartheta(\xi), \varphi(\xi)$ , and  $\Pi(\xi)$ . The range of all these factors are given as 0.1 < We < 1.2, 0.1 <  $\delta$  < 0.7, 0.1 < Nb < 0.4, 0.1 < Nt < 0.5, 1.0 < Pr < 2.5, 1.0 < Sc < 2.0, 1.0 < Pe < 2.0, 1.0 <  $\omega$  < 2.0, 1.0 < Lb < 2.0.

Figure 2(a-c) shows the variations in velocity  $(F'(\xi))$ , temperature  $(\vartheta(\xi))$ , and concentration  $(\varPhi(\xi))$  profiles via Weissenberg number (We). It is clear to note that there are two cases at all: *i.e.*, when n > 1, then it is called shear thickening case while when n < 1 then this case is called shear thickening case. It is understood that the Weissenberg number reduces the fluid velocity for the case of shear thinning, which is focused in the present analysis (Figure 2(a)). However, in general, the fluid velocity increases via the Weissenberg number for the case of shear thickening. Figure 2(b) shows the variation in  $\vartheta(\xi)$  via Weissenberg number (We). The temperature boundary thickness expands with the increasing We because the increasing We conduct low resistive force to the flow temperature and can take an infinite time to meet the ambient

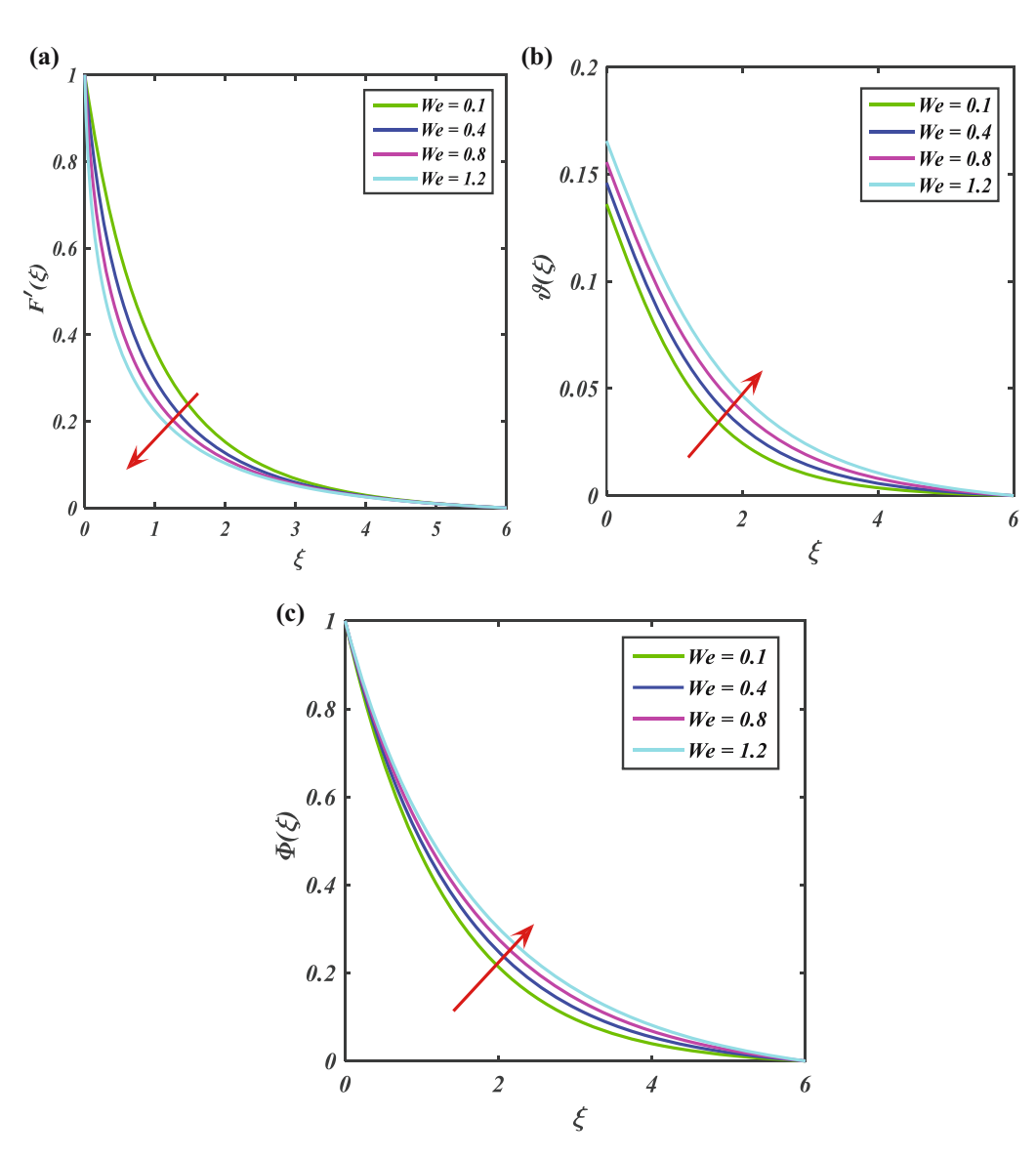


**Figure 2:** (a–c) Impact of Weissenberg number (We) on (a)  $F'(\xi)$ , (b)  $\vartheta(\xi)$ , and (c)  $\Phi(\xi)$ .

temperature. Thus, the increasing We heightens the temperature boundary layer thickness and temperature profile as well. The same is the case for the concentration profile, as shown in Figure 2(c).

Figure 3(a–c) shows the impact of curvature factor  $(\delta)$  on  $F'(\xi)$ ,  $\vartheta(\xi)$ , and  $\varPhi(\xi)$ , respectively. From these figures, we see that the higher curvature factor causes an increase in fluid velocity as well as in thermal distribution while reducing the concentration profiles. The higher curvature factor means that the cylindrical surface converts to a flat surface when  $\delta$  tends to infinity. By the fact that velocity and thermal distribution are always dominant in the case of flat surfaces as compared to the cylindrical surface. The same is the case for the velocity and thermal layer of the nanofluid flow over a cylindrical surface (Figure 3(a and b)). On the other hand, the higher curvature factor declines the concentration boundary layer thickness which declines the concentration profile of the nanofluid flow.

The significance of Brownian movement Nb over temperature profile  $\vartheta(\xi)$  and concentration of Cross-fluid  $\varPhi(\xi)$  is acknowledged in Figure 4(a and b). The intensifying magnitude of Nb strengthened the liquid temperature. Due to the increased heat generated by the random motion of nanoparticle components with varying temperatures, Nb grows and the thickness of the related thermal layers upsurges. Moreover, enhancing Nb depreciates the concentration profiles  $\varPhi(\xi)$ . Physically, Nb increases due to collisions between material particles and lowers the concentration profile.

Figure 5(a) and (b) shows the impact of Nt on  $\vartheta(\xi)$  and  $\varPhi(\xi)$ , respectively. Larger values of Nt cause improvement in both the temperature and concentration field. Physically, the thermophoresis factor plays a vital role. Thermophoretic forces are generated with increasing Nt. These forces tend to move the fluid nanoparticles from hot to colder surface regions. Due to this transport phenomenon, both the nanoparticle's concentration and temperature boundary layer

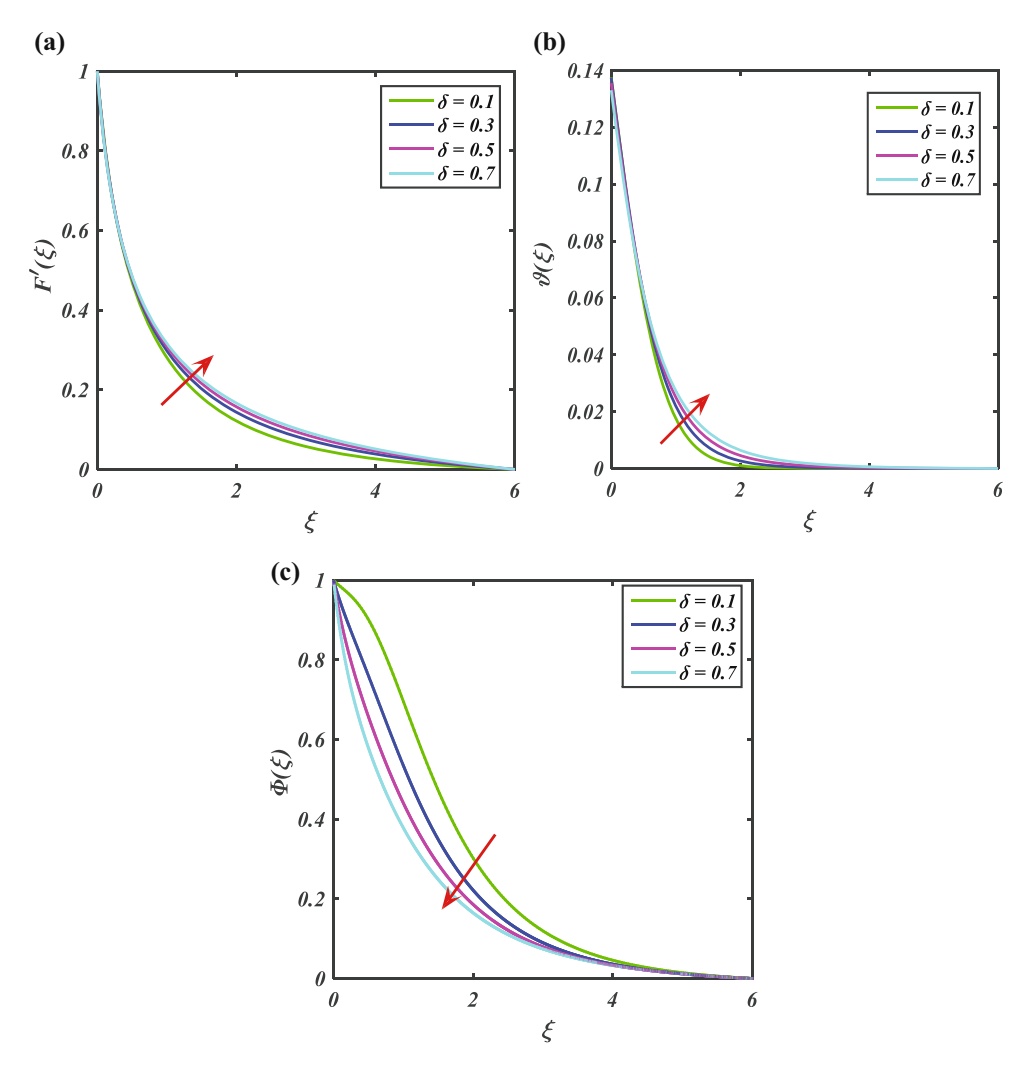


**Figure 3:** (a–c) Impact of curvature parameter  $\delta$  on (a)  $F'(\xi)$ , (b)  $\vartheta(\xi)$ , and (c)  $\Phi(\xi)$ .

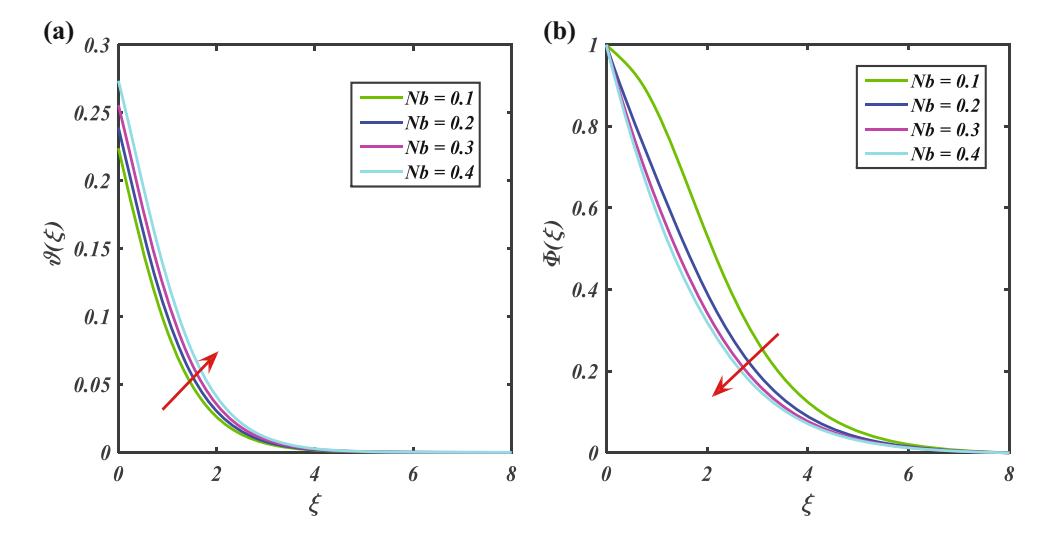


**Figure 4:** Impact of Brownian motion Nb on (a)  $\vartheta(\xi)$  and (b)  $\Phi(\xi)$ .

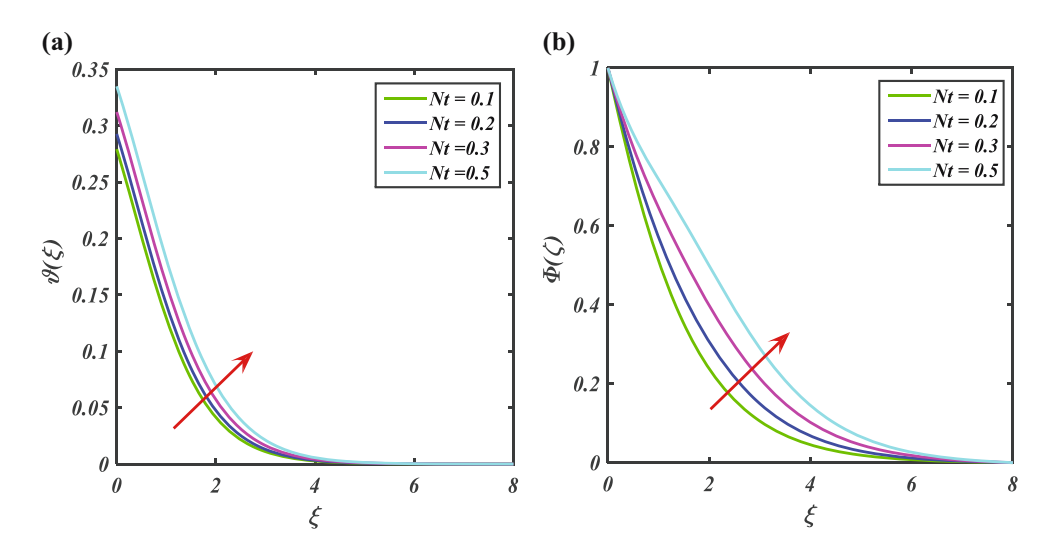


**Figure 5:** Impact of Nt on (a)  $\vartheta(\xi)$  and (b)  $\Phi(\xi)$ .

thicknesses heighten, which causes augmentation in the temperature and concentration profiles of the nanofluid flow.

Figure 6(a) shows the variation in temperature profile *via* Prandtl number (Pr). The ratio of momentum to thermal diffusivity is known as the Pr. The increasing Pr means that the momentum diffusivity is greater than the thermal diffusivity, which shows that the thermal boundary thickness reduces and, hence, the temperature profile reduces. Thus, a decreasing impact in the temperature profile *via* Pr is perceived. Figure 6(b) shows the impact of Sc on the concentration profile. The higher the Sc, the lower the concentration profile. Actually, the higher Sc means the low Brownian diffusivity, which results in a reduction in the concentration boundary layer thickness. Thus, a higher Sc

decays the concentration boundary layer thickness and concentration profile as well.

For higher estimates of (Lb), Figure 7(a) shows the deprecation in the motile density. Physically, when (Lb) is greater, as microorganisms are less likely to move through a fluid, so  $\Pi(\xi)$ goes down. Figure 7(b) makes it easy to see that when (Pe) grows,  $\Pi(\xi)$  decreases. Since the diffusivity of higher (Pe) microorganisms diminishes, so does the thickness of the corresponding layer. To verify the impact of  $(\omega)$  on microbial concentration  $\Pi(\xi)$ , Figure 7(c) is sketched. We found that as the temperature of cross-fluid has increased, its viscosity  $(\omega)$  decreased. Motile density decreases as the concentration of microorganisms in ambient fluids grows with  $\omega$ .

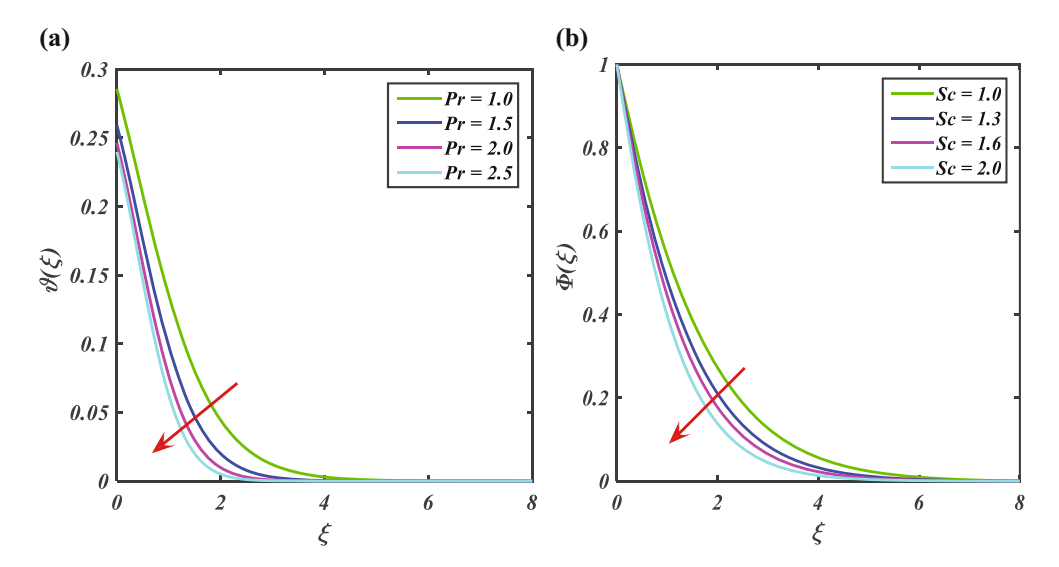


**Figure 6:** Impact of Pr on (a)  $\vartheta(\xi)$  and (b)  $\varPhi(\xi)$ .

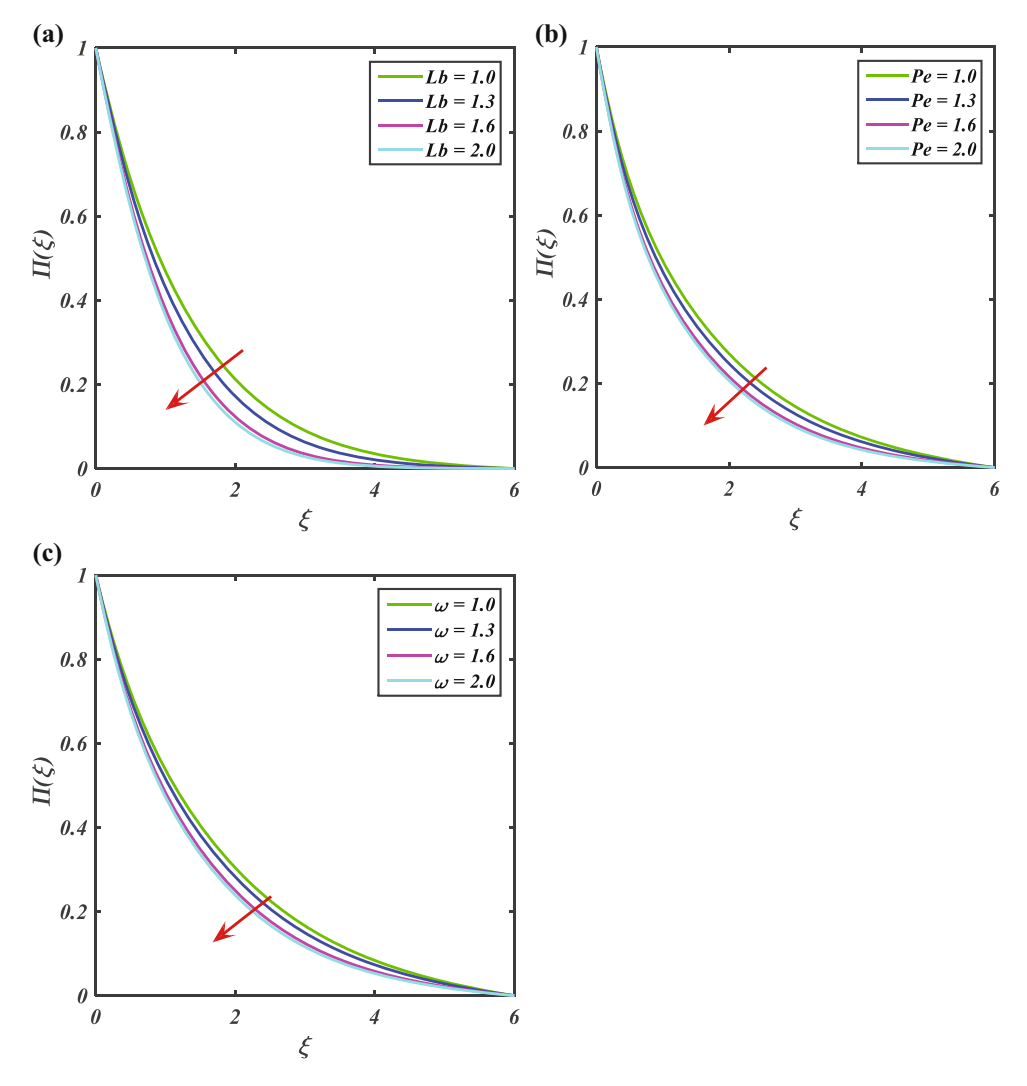


**Figure 7:** (a) Impact of Lb on  $\Pi(\xi)$ , (b) impact of Pe on  $\Pi(\xi)$ , and (c) impact of  $\omega$  on  $\Pi(\xi)$ .

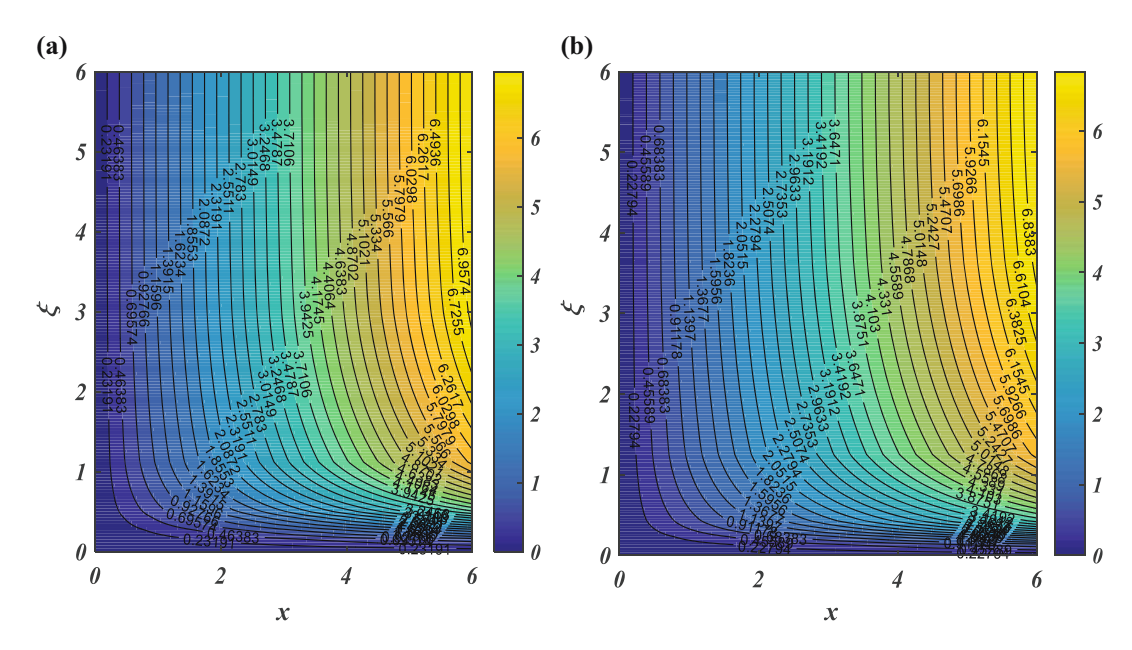


Figure 8: Contour plot for (a) mixed convective flow and (b) without mixed convective flow.

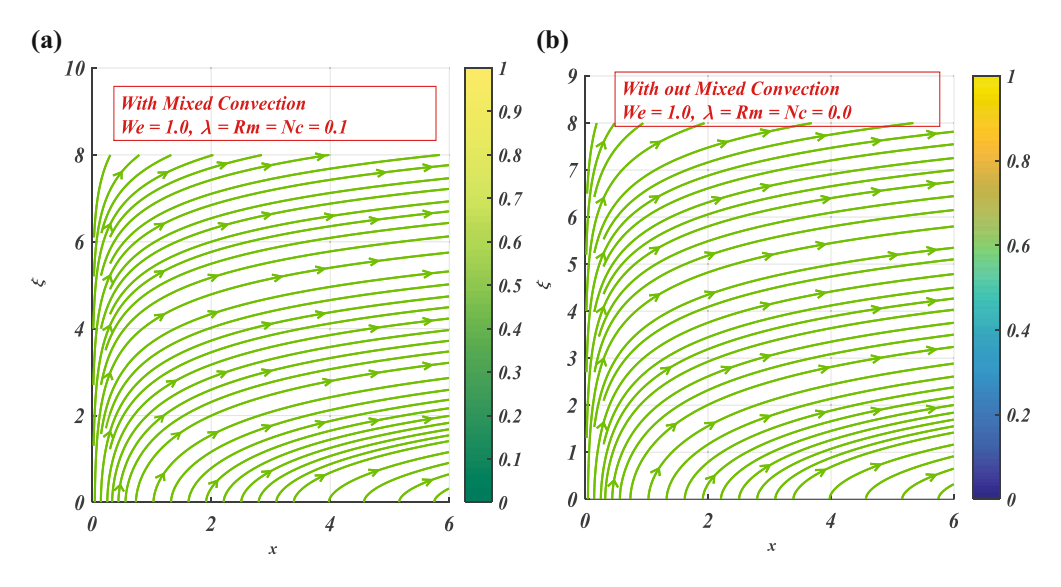


Figure 9: Streamline for the (a) mixed convective and (b) without mixed convective.

Figure 8(a and b) shows the contour graphs for fluid flow with and without mixed convection characteristics. Greater values of mixed convective parameters get larger in the pattern of flow and cause enhanced viscosity of the fluid. Figure 9(a and b) shows streamlines created at various values assigned to We,  $\lambda$ , Rm, and Nc. For larger values, flow is enhanced more rapidly and is moved away from the origin.

Table 1 consists of the comparison of our results with published work. Table 2 summarizes the data of skin friction measured at a cylindrical surface. From this table, it has been noticed that when We and  $\delta$  are increased, skin

**Table 1:** Comparative analysis of  $\vartheta'(0)$  when Nb = 0, Nt = 0, Rd = 0

Pr	Bidin and Nazar [47]	Rafique <i>et al.</i> [48]	Current result		
1	0.9548	0.9548	0.95481		
2	1.4714	1.4714	1.86912		
3	1.8691	1.8691	1.86915		

friction is reduced, but when  $\lambda$  is increased, skin friction is escalated. Greater values of the dimensionless parameters Rd, Nt, Nb, Pe, Lb, Pr, and Sc reduced the heat, mass, and motile microorganism density, as observed in Tables 3–5.

12 — Humaira Yasmin et al. DE GRUYTER

**Table 2:** Numeric data for Skin friction against variations in various factors

**Table 4:** Numeric data of Sherwood number against variations in various factors

S	We	λ	Nc	Rm	$Re_{x}^{1/2} Cf$	Nb	Nt	Kr	δ	Sc	-Re <sup>1/2</sup> Sh
1.1	0.5	0.1	0.1	0.1	1.6861	1.1	0.5	1	0.1	0.3	1.1623
1.3					1.6341	1.6					0.9809
.5					1.6027	2.1					0.8970
.8					1.5599	2.6					0.8495
	1				1.9861		1				1.2250
	1.4				0.9012		1.4				1.0350
	1.6				0.7345		1.6				0.9809
	1.9				0.5783		1.9				0.9244
	1.0	0.2			1.6920			1.1			1.1517
		1.2			1.7464			1.2			1.4243
		2.1			1.7897			1.3			1.5415
		3.2			1.8353			1.4			1.6997
			0.1		3.4716				0.1		1.1845
			0.3		3.1512				0.3		1.2180
			0.5		2.8879				0.5		1.2531
			0.7		2.6659				0.7		1.2831
				0.1	2.6239					1.1	1.4840
				0.3	2.5041					1.3	1.4978
				0.5	2.3949					1.5	1.5117
				0.7	2.2949					1.7	1.5255

**Table 3:** Numeric data for Nusselt number against variations in various factors

**Table 5:** Numeric data of motile density against variations in various factors

Nb	Nt	Pr	δ	Rd	-Re <sup>1/2</sup> Nu	Pe	Lb	ω	δ	Sc	-Re <sup>1/2</sup> Nh
0.1	0.5	1	0.1	0.3	0.2073	1.1	0.5	1	0.1	0.3	2.5994
0.3					0.1980	1.6					2.5362
0.5					0.1840	2.1					2.4665
8.0					0.1702	2.6					2.3909
	1				0.1389		1				2.5994
	1.4				0.1276		1.4				2.6109
	1.6				0.1116		1.6				2.6221
	1.9				0.1056		1.9				2.6332
		0.3			0.1583			1.1			3.6269
		1.2			0.1470			1.2			3.7781
		2.1			0.1348			1.3			3.9266
		3.2			0.1218			1.4			4.0750
			0.1		0.3098				0.1		3.5144
			0.3		0.2949				0.3		3.5487
			0.5		0.2891				0.5		3.5863
			0.7		0.2722				0.7		3.6238
				0.1	0.3498					1.1	3.4617
				0.3	0.3349					1.3	3.4428
				0.5	0.3291					1.5	3.4066
				0.7	0.3143					1.7	3.4046

DE GRUYTER Thermal radiative flow — 13

# 4 Conclusion

The influence of linearly radiative and bio-convective crossnanofluid flow across a vertical cylinder under convective conditions at the boundary is investigated numerically. The heat and mass transfer features of nanofluids are shown in the associated tables and figures. Below is a list of some salient points:

- Growth in We reduces the velocity profiles while an upsurge in  $\delta$  boosts the velocity curve.
- As the curvature parameter is increased, the velocity field and temperature field decreased, close to the surface of the cylinder.
- The temperature has increased for both Brownian movement and thermophoresis force, whereas these variables behave differently on the concentration profiles.
- The temperature and concentration fields of nanoparticles are diminished by augmentation in the Pr and the Sc, while growth in B<sub>i</sub> enhances the temperature profiles.
- Upsurge in the Peclet number decays the microorganism density profiles.
- Increases in the curvature parameter and the Weissenberg number caused skin friction to decrease.
- The Sherwood number declines with the escalation in the chemical reaction and the Sc.

**Acknowledgments:** The authors extend their appreciation to the Deanship of Scientific Research at King Khalid University, Abha, Saudi Arabia, for funding this work through the Research Group Project under Grant No. RGP.1/505/44. This work was supported by the Deanship of Scientific Research, the Vice Presidency for Graduate Studies and Scientific Research, King Faisal University, Saudi Arabia (Grant No. 4475).

**Funding information:** This work was funded through the Deanship of Scientific Research at King Khalid University, Abha, Saudi Arabia, the Research Group Project under Grant Number RGP.1/505/44. This work was supported by the Deanship of Scientific Research, the Vice Presidency for Graduate Studies and Scientific Research, King Faisal University, Saudi Arabia (Grant No. 4475).

**Author contributions:** All authors have accepted responsibility for the entire content of this manuscript and approved its submission.

**Conflict of interest:** The authors state no conflict of interest.

**Data availability statement:** All data generated or analyzed during this study are included in this published article (and its supplementary information files).

# References

- [1] Hosseinzadeh J, Roghani S, Mogharrebi AR, Asadi A, Waqas M, Ganji DD, et al. Investigation of cross-fluid flow containing motile gyrotactic microorganisms and nanoparticles over a three-dimensional cylinder. Alex Eng J. 2020;59:3297–307.
- [2] Ali M, Sultan F, Khan WA, Shahzad M, Arif H. Important features of expanding/contracting cylinder for Cross magneto-nanofluid flow. Chaos Solit Fractal. 2020;133:109656.
- [3] Xiao Q, Cheng J, Zhang B, Zhou J, Chen W. Schlieren visualization of the interaction of jet in crossflow and deflagrated flame in hydrogen-air mixture. Fuel. 2021;292:120380.
- [4] Azam M, Xu T, Khan M. Numerical simulation for variable thermal properties and heat source/sink in flow of Cross nanofluid over a moving cylinder. Int Commun Heat Mass Transf. 2020;118:104832.
- [5] Zhang G, Si Z, Zhai C, Luo H, Ogata Y, Nishida K, et al. Characteristics of wall-jet vortex development during fuel spray impinging on flatwall under cross-flow conditions. Fuel. 2022;317:123507.
- [6] Khan U, Zaib A, Bakar SA, Ishak A, Baleanu D, Sherif ESM, et al. Computational simulation of cross-flow of Williamson fluid over a porous shrinking/stretching surface comprising hybrid nanofluid and thermal radiation. AIMS Math. 2022;7(4):6489–515.
- [7] Khosravi M, Javan M. Three-dimensional features of the lateral thermal plume discharge in the deep cross-flow using dynamic adaptive mesh refinement. Theor Comput Fluid Dyn. 2022;36(3):405–22.
- [8] Sarbazi Z, Hormozi F. Numerical study of entropy generation and forced convection heat transfer of a nanofluid in a channel with different fin cross-sections. Int J Numer Method Heat Fluid Flow. 2022;32(1):62–98.
- [9] Darvesh A, Altamirano GC, Salas SAH, Sánchez Chero M, Carrión Barco G, Bringas Salvador JL, et al. Infinite shear rate viscosity model of cross fluid flow containing nanoparticles and motile gyrotactic microorganisms over 3-D cylinder. J Nanofluids. 2023;12(4):930–41.
- [10] Choi SU, Eastman JA. Enhancing thermal conductivity of fluids with nanoparticles (No. ANL/MSD/CP-84938; CONF-951135-29). Argonne National Lab. (ANL): Argonne, IL, United States; 1995.
- [11] Dinarvand S, Berrehal H, Pop I, Chamkha AJ. Blood-based hybrid nanofluid flow through converging/diverging channel with multiple slips effect: a development of Jeffery-Hamel problem. Int J Numer Method Heat Fluid Flow. 2023;33(3):1144–60.
- [12] Shamshuddin MD, Akkurt N, Saeed A, Kumam P. Radiation mechanism on dissipative ternary hybrid nanoliquid flow through rotating disk encountered by Hall currents: HAM solution. Alex Eng J. 2023;65:543–59.
- [13] Madhukesh JK, Sarris IE, Prasannakumara BC, Abdulrahman A. Investigation of thermal performance of ternary hybrid nanofluid flow in a permeable inclined cylinder/plate. Energies. 2023;16(6):2630.
- [14] Nanda P, Sandeep N, Sulochana C, Ashwinkumar GP. Enhanced heat transmission in methanol-based AA7072/AA7075 tangent hyperbolic hybrid nanofluid flow along a nonlinear expandable surface. Numer Heat Transf A-Appl. 2023;83(7):711–25.
- [15] Sharma P, Said Z, Kumar A, Nizetic S, Pandey A, Hoang AT, et al. Recent advances in machine learning research for nanofluid-based heat transfer in renewable energy system. Energy Fuels. 2022;36(13):6626–58.
- [16] Mohammed HA, Bhaskaran G, Shuaib NH, Saidur R. Heat transfer and fluid flow characteristics in microchannels heat exchanger using nanofluids: a review. Renew Sustain Energy Rev. 2011;15(3):1502–12.

- [17] Khan A, Alyami MA, Alghamdi W, Alqarni MM, Yassen MF, Tag Eldin E, et al. Thermal examination for the micropolar gold–blood nanofluid flow through a permeable channel subject to gyrotactic microorganisms. Front Energy Res. 2022;10:993247.
- [18] Khan A, Iqbal Z, Ahammad NA, Sidi MO, Elattar S, Awad S, et al. Bioconvection Maxwell nanofluid flow over a stretching cylinder influenced by chemically reactive activation energy surrounded by a permeable medium. Front Phys. 2023;10:1348.
- [19] Bhatti MM, Ellahi R. Numerical investigation of non-Darcian nanofluid flow across a stretchy elastic medium with velocity and thermal slips. Numer Heat Tr A-Appl Fund. 2023;83(5):323–43.
- [20] Mahmood Z, Iqbal Z, Alyami MA, Alqahtani B, Yassen MF, Khan U, et al. Influence of suction and heat source on MHD stagnation point flow of ternary hybrid nanofluid over convectively heated stretching/shrinking cylinder. Adv Mech Eng. 2022;14(9):16878132221126278.
- [21] Li J, Wang B, Qiu X, Wu J, Zhou Q, Fu S, et al. Three-dimensional vortex dynamics and transitional flow induced by a circular cylinder placed near a plane wall with small gap ratios. J Fluid Mech. 2022;953.
- [22] Pattnaik PK, Mishra SR, Bég OA, Khan UF, Umavathi JC. Axisymmetric radiative titanium dioxide magnetic nanofluid flow on a stretching cylinder with homogeneous/heterogeneous reactions in Darcy-Forchheimer porous media: Intelligent nanocoating simulation. Mater Sci Eng B. 2022;277:115589.
- [23] Reddy YD, Goud BS, Nisar KS, Alshahrani B, Mahmoud M, Park C. Heat absorption/generation effect on MHD heat transfer fluid flow along a stretching cylinder with a porous medium. Alex Eng J. 2023;2023(64):659–66.
- [24] Othman A, Ali H, Jubair B, Yahya Almusawa MM, Aldin S. Numerical simulation of the nanofluid flow consists of gyrotactic microorganism and subject to activation energy across an inclined stretching cylinder. Sci Rep. 2023;13(1):7719.
- [25] Shaheen N, Ramzan M, Kadry S, Abbas M, Saleel CA. Bioconvective unsteady fluid flow across concentric stretching cylinders with thermal-diffusion and diffusion-thermo effects. Numer Heat Tr A-Appl. 2023;2020:1–17.
- [26] Ahmad B, Ahmad MO, Farman M, Akgül A, Riaz MB. A significance of multi slip condition for inclined MHD nano-fluid flow with non linear thermal radiations, Dufuor and Sorrot, and chemically reactive bio-convection effect. S Afr J Chem Eng. 2023;43:135–45.
- [27] Liu Z, Li S, Sadaf T, Khan SU, Alzahrani F, Khan MI, et al. Numerical bio-convective assessment for rate type nanofluid influenced by Nield thermal constraints and distinct slip features. Case Stud Therm Eng. 2023;44:102821.
- [28] Fathollahi R, Alizadeh AA, Safari Y, Nabi H, Shamsborhan M, Taghinia F. Examination of bio convection with nanoparticles containing microorganisms under the influence of magnetism fields on vertical sheets by five-order Runge-Kutta method. Heliyon. 2023;9(5):e15982.
- [29] Kada B, Hussain I, Pasha AA, Khan WA, Tabrez M, Juhany KA, et al. Significance of gyrotactic microorganism and bioconvection analysis for radiative Williamson fluid flow with ferromagnetic nanoparticles. Therm Sci Eng Prog. 2023;39:101732.
- [30] Saraswathy M, Prakash D, Muthtamilselvan M, Al-Mdallal QM. Theoretical study on bio-convection of micropolar fluid with an

- exploration of Cattaneo-Christov heat flux theory. Int J Mod Phys B. 2023;2450016.
- [31] Chu YM, Khan MI, Khan NB, Kadry S, Khan SU, Tlili I, et al. Significance of activation energy, bio-convection and magnetohydrodynamic in flow of third grade fluid (non-Newtonian) towards stretched surface: A Buongiorno model analysis. Int Commun Heat Mass Transf. 2020;118:104893.
- [32] Hussain Z, Alam MM, Pasha AA, Khan WA, Ali M, Khan AI, et al. Gyrotaticmicroorganisms analysis for radiative 3D Carreau nanofluid flow configured by activation energy and viscous dissipation. Therm Sci Eng Prog. 2023;2023(42):101898.
- [33] Yu D, Wang R. An optimal investigation of convective fluid flow suspended by carbon nanotubes and thermal radiation impact. Mathematics. 2022;10(9):1542.
- [34] Huang Y, Xiao X, Kang H, Lv J, Zeng R, Shen J. Thermal management of polymer electrolyte membrane fuel cells: A critical review of heat transfer mechanisms, cooling approaches, and advanced cooling techniques analysis. Energy Convers Manag. 2022;254:115221.
- [35] Said Z, Arora S, Farooq S, Sundar LS, Li C, Allouhi A. Recent advances on improved optical, thermal, and radiative characteristics of plasmonic nanofluids: Academic insights and perspectives. Sol Energy Mater Sol Cells. 2022;236:111504.
- [36] Dharmaiah G, Mebarek-Oudina F, Kumar MS, Kala KC. Nuclear reactor application on Jeffrey fluid flow with Falkner-skan factor, Brownian and thermophoresis, non linear thermal radiation impacts past a wedge. J Indian Chem Soc. 2023;100(2):100907.
- [37] Suresh Kumar Y, Hussain S, Raghunath K, Ali F, Guedri K, Eldin SM, et al. Numerical analysis of magnetohydrodynamics Casson nanofluid flow with activation energy, Hall current and thermal radiation. Sci Rep. 2023;13(1):4021.
- [38] Pandey AK, Bhattacharyya K, Gautam AK, Rajput S, Mandal MS, Chamkha AJ, et al. Insight into the relationship between non-linear mixed convection and thermal radiation: The case of Newtonian fluid flow due to non-linear stretching. Propuls Power Res. 2023;12(1):153–65.
- [39] Alrehili M. Improvement for engineering applications through a dissipative Carreau nanofluid fluid flow due to a nonlinearly stretching sheet with thermal radiation. Case Stud Therm Eng. 2023;2023(42):102768.
- [40] Sharma BK, Kumar A, Gandhi R, Bhatti MM, Mishra NK. Entropy generation and thermal radiation analysis of EMHD Jeffrey nanofluid flow: Applications in solar energy. Nanomaterials. 2023;13(3):544.
- [41] Cross MM. Rheology of non-Newtonian fluids: a new flow equation for pseudoplastic systems. J Colloid Sci. 1965;20(5):417–37.
- [42] Rehman M, Israr UrHC, Aamir H, Sajid Q, Wasim J, Zehba R, et al. Soret and dufour influences on forced convection of cross radiative nanofluid flowing via a thin movable needle. Sci Rep. 2022;12(1):18666.
- [43] Azam M, Shakoor A, Rasool HF, Khan M. Numerical simulation for solar energy aspects on unsteady convective flow of MHD Cross nanofluid: A revised approach. Int J Heat Mass Transf. 2019:131:495–505.
- [44] Yao L, Grishaev A, Cornilescu G, Bax A. The impact of hydrogen bonding on amide 1H chemical shift anisotropy studied by crosscorrelated relaxation and liquid crystal NMR spectroscopy. J Am Chem Soc. 2010;132(31):10866–75.

- [45] Khan MI, Hayat T, Khan MI, Alsaedi A. Activation energy impact in nonlinear radiative stagnation point flow of Cross nanofluid. Int Commun Heat Mass Transf. 2018;91:216–24.
- [46] Sharma RP, Mishra SR. Effect of higher order chemical reaction on magnetohydrodynamic micropolar fluid flow with internal heat source. Int J Fluid Mech Res. 2020;47(2).
- [47] Bidin B, Nazar R. Numerical solution of the boundary layer flow over an exponentially stretching sheet with thermal radiation. Eur J Sci Res. 2009;33:710–7.
- [48] Rafique K, Alotaibi H, Ibrar N, Khan I. Stratified flow of micropolar nanofluid over riga plate: Numerical analysis. Energies. 2022;15:316.